Research Article

Chaotic Extension Neural Network-Based Fault Diagnosis Method for Solar Photovoltaic Systems

Kuo-Nan Yu, Her-Terng Yau, and Jian-Yu Li

Department of Electrical Engineering, National Chin-Yi University of Technology, No. 57, Section 2, Zhongshan Road, Taiping District, Taichung 41170, Taiwan

Correspondence should be addressed to Her-Terng Yau; pan1012@ms52.hinet.net

At present, the solar photovoltaic system is extensively used. However, once a fault occurs, it is inspected manually, which is not economical. In order to remedy the defect of unavailable fault diagnosis at any irradiance and temperature in the literature with chaos synchronization based intelligent fault diagnosis for photovoltaic systems proposed by Hsieh et al., this study proposed a chaotic extension fault diagnosis method combined with error back propagation neural network to overcome this problem. It used the nn toolbox of matlab 2010 for simulation and comparison, measured current irradiance and temperature, and used the maximum power point tracking (MPPT) for chaotic extraction of eigenvalue. The range of extension field was determined by neural network. Finally, the voltage eigenvalue obtained from current temperature and irradiance was used for the fault diagnosis. Comparing the diagnostic rates with the results by Hsieh et al., this scheme can obtain better diagnostic rates when the irradiances or the temperatures are changed.

1. Introduction

This study focused on solar photovoltaic fault diagnosis. Solar energy is generated from the sunlight, which is an inexhaustible renewable energy, as compared to other green energies. At present, the solar photovoltaic system has been used in many fields, and current research focuses are the use of this technology, such as efficient storage, environmental issues, and subsequent maintenance. The analysis based on fault diagnosis technology can save labor cost greatly.

Many studies have proposed fault diagnosis technologies for photovoltaic system. Most of traditional fault diagnosis technologies are based on intelligent algorithms including neural network [1–3]. For example, in 2009, Wu et al. used BP neural network for fault diagnosis, the diagnostic rate was very high, but a large amount of data was required for learning and training. The convergence of samples was time consuming [4]. In 2011, Syafaruddin et al. used three-layer artificial neural network for fault diagnosis and provided more accurate diagnostic result than one-layer fault diagnosis. However, this method was also time consuming [5]. In 2011, Shimakage et al. discussed photovoltaic system fault diagnosis and used measurement and observation for diagnosis. They recorded the power generated by the faulted photovoltaic system and compared it with the presently measured power. However, the data for comparison were required and time was required to create the database [6]. In 2012, Zhao et al. proposed a decision tree-based diagnostic method for photovoltaic cell. The diagnostic rate of this method was as high as 99.8%, but more than 1,000 times of intercomparison were required in the course of diagnosis [7]. In 2014, Tadj et al. proposed a GISTEL (gisement solaire par télédétection: solar radiation by teledetection) model to improve the photovoltaic cell diagnosis on fuzzy logic estimated satellite image. The method was difficult to be implemented [8]. In 2014, Hsieh et al. used chaotic extension theory for diagnosis, and the accuracy rate was very high. However, due to the limitation of extension theory, the diagnostic rate decreased greatly when the temperature and irradiance changed. This study aims to remedy the defects in the literature [9].

In the literature [9], 10-series 2-parallel solar photovoltaic array was used as the model of fault diagnosis. Chaotic synchronization system was combined with extenics for fault diagnosis. However, the classical domain cannot identify
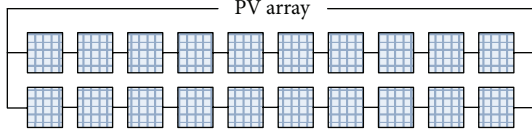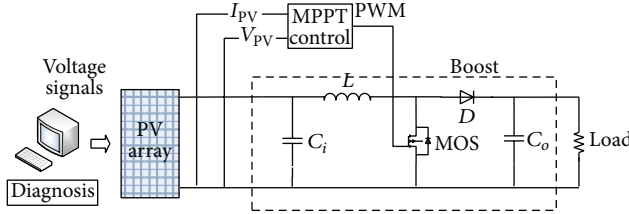
Figure 1: 10-series 2-parallel schematic diagram.

Figure 2: MPPT control system schematic diagram.

Table 1: Solar panel model and specifications.

Solar panel model	SM 1611
Maximum power (P_{MAX})	1.65 W
Open-circuit voltage (V_{OC})	3.0 V
Short-circuit current (I_{SC})	0.8 A

Table 2: Solar photovoltaic system fault category.

Fault category	Fault condition (short circuit set in faulted solar cell)
Case 1 (C1)	There is no fault in two-series connected photovoltaic cells.
Case 2 (C2)	One solar cell fault occurs in any series branch of two-series branch photovoltaic system.
Case 3 (C3)	Two solar cells have faults in any series branch of two-series branch photovoltaic system.
Case 4 (C4)	Three solar cells have faults in any series branch of two-series branch photovoltaic system.
Case 5 (C5)	One solar cell fault occurs in both of the two-series branches of two-series branch photovoltaic system.
Case 6 (C6)	Two solar cells have faults in both of the two-series branches of two-series branch photovoltaic system.
Case 7 (C7)	In the two-series branch photovoltaic system, one solar cell has fault in one-series branch and two solar cells have faults in the other branch.
Case 8 (C8)	In the two-series branch photovoltaic system, one solar cell has fault in one-series branch and four solar cells have faults in the other branch.
Case 9 (C9)	In the two-series branch photovoltaic system, two solar cells have faults in one-series branch and three solar cells have faults in the other branch.

the fault state accurately as long as the irradiance and temperature have changed. This study uses BP neural network, so as to remedy the defect of unavailable diagnosis when the irradiance and temperature change, and uses the center of error dynamic trajectories of two chaotic subsystems as eigenvalue, to overcome the decrease in diagnostic rate that resulted from undervoltage at low light level.

2. Architecture of Solar Power System

The fault diagnosis module used in this paper is 10-series 2-parallel photovoltaic, as shown in Figure 1, and MPPT, the system architecture, is shown in Figure 2; the matlab 2010 is used for simulation. The specifications of SM1611 photovoltaic cell are shown in Table 1 [9].

The photovoltaic cell is set as short circuit to simulate nine fault states to be illustrated by Table 2, and the I-V and P-V characteristic curves at different irradiances and temperatures are observed.

3. Research Method

3.1. Chaos Synchronization Theory. The chaos synchronization theory designs a slave system to synchronize a master system. The chaos synchronization system consists of two subsystems, a master system and a slave system, representing the relation between master and servant. This paper uses Lorenz chaos synchronization system, which is highly sensitive to parametric variation, to capture the voltage signal of photovoltaic system and extract the kinematic trajectory of dynamic error. The center of this kinematic trajectory is used

as the eigenvalue of fault. The architecture of Lorenz chaos synchronization system is expressed as follows [10]:

$$\text{Master:} \begin{cases} \dot{x}_1 = \alpha\left(x_2 - x_1\right) \\ \dot{x}_2 = \beta x_1 - x_1 x_3 - x_2 \\ \dot{x}_3 = x_1 x_2 - \gamma x_3, \end{cases}$$

$$\text{Slave:} \begin{cases} \dot{y}_1 = \alpha\left(y_2 - y_1\right) \\ \dot{y}_2 = \beta y_1 - y_1 y_3 - y_2 \\ \dot{y}_3 = y_1 y_2 - \gamma y_3, \end{cases} \tag{1}$$

where α, β, and γ are system parameters and x and y are the state variables. The master-slave system error state can be expressed as $e_1 = x_1 - y_1$, $e_2 = x_2 - y_2$, and $e_3 = x_3 - y_3$; the dynamic error system is expressed as follows [10]:

$$\begin{bmatrix} \dot{e}_1 \\ \dot{e}_2 \\ \dot{e}_3 \end{bmatrix} = \begin{bmatrix} -\alpha & \alpha & 0 \\ \beta & -1 & 0 \\ 0 & 0 & -\gamma \end{bmatrix} \begin{bmatrix} e_1 \\ e_2 \\ e_3 \end{bmatrix} + \begin{bmatrix} 0 \\ -x_1 x_3 + y_1 y_3 \\ x_1 x_2 - y_1 y_2 \end{bmatrix}. \tag{2}$$

This paper uses the final dynamic errors $\dot{e}_1$, $\dot{e}_2$, and $\dot{e}_3$ to draw the dynamic error trajectory diagram for observation.

3.2. Extension Theory. The extension theory solves contradiction problem quantitatively and qualitatively to change it into compatibility problem. The difference between extension theory and fuzzy theory is that the range of fuzzy set is $\langle 0, 1 \rangle$, whereas the extension is a real number extended from $\langle 0, 1 \rangle$ to $\langle -\infty, \infty \rangle$ [11]. The extension theory is characterized by a small amount of calculation and simplicity, and it has high accuracy rate in evaluating multiple parameters and complex construction. This paper uses this feature to judge
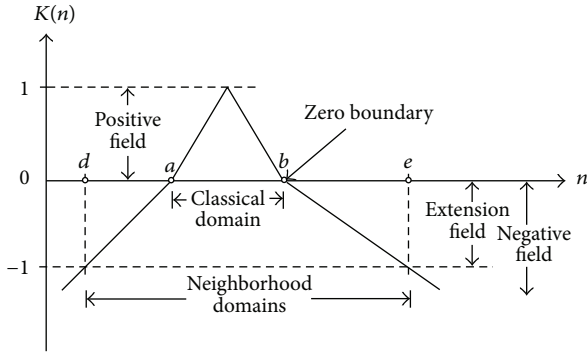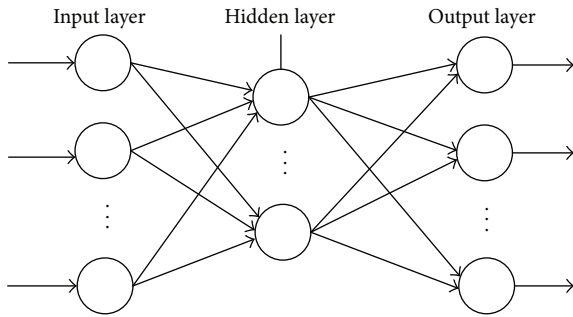
FIGURE 3: Extension set correlation function.

FIGURE 4: Neural network architecture.

the eigenvalue captured by Lorenz chaos synchronization system to identify the fault category of photovoltaic system.

3.2.1. Matter-Element Theory. In the extension theory, the matter-element is the basic element describing things. The general matter-element model is the mathematical model applied to extension, defined as follows [12]:

$$R(P, C, V) = \begin{bmatrix} P & c_1 & v_1 \\ & c_2 & v_2 \\ & \vdots & \vdots \\ & c_n & v_n \end{bmatrix}, \quad (3)$$

where R is the matter-element, P is the name of the matter-element, C is the eigenvector, and V is the magnitude vector corresponding to C.

3.2.2. Extension Set. The extension set means the range of set is extended from $-\infty$ to ∞ to represent the extensibility of thing characteristics, the correlation function is defined as (4), and the correlation grade of extension set can be expressed as Figure 3 [13].

Consider

$$K(n) = \frac{\rho(n, N_o)}{D(n, N_o, N_p)}$$

$$D(n, N_o, N_p) = \begin{cases} \rho(n, N_p) - \rho(n, N_o), & n \notin N_o \\ -1, & n \in N_o \end{cases}$$
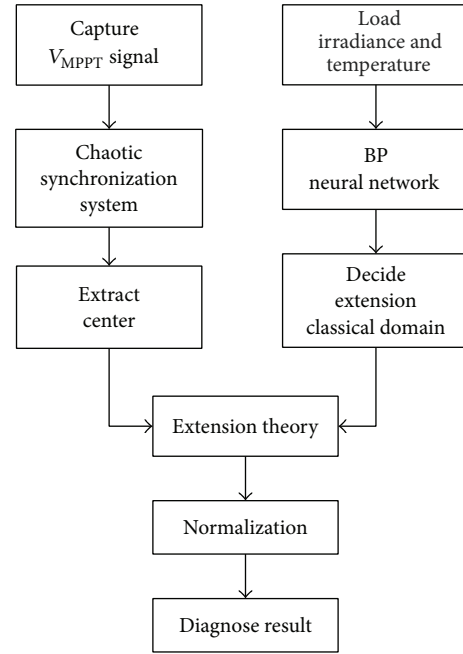

FIGURE 5: System diagnosis process of chaotic extension neural network.

$$\rho(n \cdot N_o) = \left| n - \frac{a+b}{2} \right| - \frac{b-a}{2}$$

$$\rho(n \cdot N_p) = \left| n - \frac{d+e}{2} \right| - \frac{e-d}{2},$$

$$(4)$$

where K is the correlation grade, N_o is the classical domain, N_s is the neighborhood domain, and $N_o \in N_s$.

3.3. Neural Network. The neural network is a computational theory derived from human brain structure, and it consists of many layers of neurons. The neural network is capable of calculation, memorization, reasoning, and logical decision and readjustment. The forward error backpropagation algorithm proposed by Rvomelhart and Mcclelland (1986) has excellent effect on computing nonlinear system. This paper uses this feature to calculate the eigenvalue changed at different temperatures and irradiances and uses BP neural network to determine the classical domain and neighborhood domain of extension theory.

The neural network consists of multiple layers of neurons; the input end is called input layer and the output end is called output layer. The hidden layer is between the output layer and input layer. The input layer and the output layer are the basic structures forming the neural network; the hidden layer is dispensable. The basic structure is shown in Figure 4 [14].

3.4. Chaotic Extension Neural Network Diagnosis System and Process. Figure 5 shows the system diagnosis process of chaotic extension neural network. First, the measured irradiance, temperature, and V_{MPPT} are recorded, and the recorded irradiance and temperature are imported into the BP neural
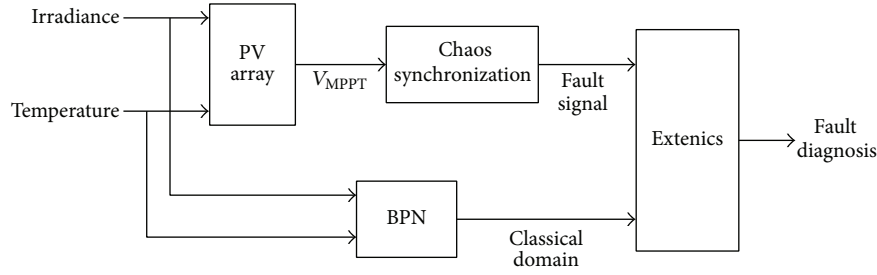
Figure 6: Schematic diagram of system diagnosis of chaotic extension neural network.
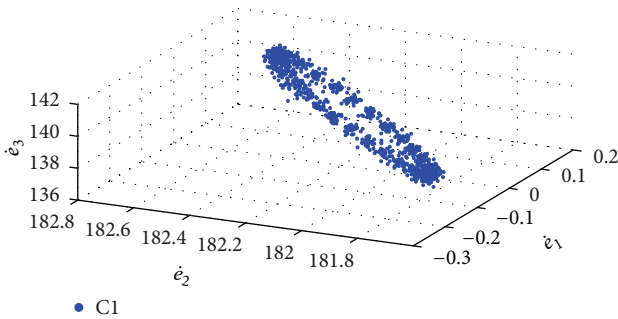

Figure 7: Three-dimensional diagram of normal chaotic dynamic error at 500 W/m² 40°C.

Table 3: Sunshine intensity in different time intervals.

Time interval (UTC + 08:00)	Irradiance value (W/m²)
7:00~8:00	158~395
8:00~9:00	395~656
9:00~10:00	656~730
10:00~11:00	730~870
11:00~12:00	870~932
12:00~13:00	870~914
13:00~14:00	870~913
14:00~15:00	870~912
15:00~16:00	632~870
16:00~17:00	158~280

network system to obtain the extension classical domain range of chaos center eigenvalue at current irradiance and temperature, and then the recorded voltage is imported into the chaos synchronization system to obtain a kinematic trajectory of chaotic dynamic system. The center point of kinematic trajectory is taken as the basis of diagnosis. Finally, the fault category of photovoltaic system can be identified as long as the obtained signal is imported into the diagnostic system of chaotic extension neural network.

4. Simulation Results and Comparison

This study aims to remedy the defect of unavailable diagnosis at varying irradiance and temperature in the literature [9], so the BP neural network is adopted. Figure 6 is the schematic diagram of system diagnosis.

4.1. Simulation Results. This study uses matlab 2010 and nn toolbox for simulation. The fault category is the short circuit in the solar panel of photovoltaic array, so as to simulate one normal state and eight fault states (i.e., C1~C9), as shown in Table 2.

The P-V and I-V characteristic curves are different in different states. The additional noise makes the kinematic trajectory of chaos system easier to be identified. Figure 7 is the three-dimensional diagram of chaotic dynamic error in the normal state of 500 W/m² 40°C; the chaos center points in various states are taken as the range of extension classical domain, and the BP neural network is used to decide the chaos center points at different temperatures and irradiances.

The sunshine intensity is about 400 W/m² ~ 1000 W/m² during 8:00~16:00 in Taiwan, as shown in Table 3 [15], and the temperature is about 25°C~50°C; the simulation is based on the conditions [9]. Figures 8(a), 8(b), 9(a), and 9(b) show the P-V and I-V characteristic curves at 1000 W/m² 25°C and 500 W/m² 40°C.

First, the irradiance of 400 W/m² ~ 1000 W/m² is divided into intervals of 100 irradiance; the temperature is divided into 25°C, 30°C, 40°C, and 50°C intervals as the input ends of BP neural network. The voltage of each interval is taken for chaos signal extraction; the obtained signal center point is used as the output end of neural network. Figures 10 and 11 show the $\dot{e}_1 - \dot{e}_3$ dynamic error plane and center of different faults at 1000 W/m² 25°C and 500 W/m² 40°C. The data of $\dot{e}_3$ center point of each interval are obtained. Table 4 shows the center point values at various irradiances and temperatures. The data are imported into the BP neural network of nn tool for training to calculate the center point of chaotic kinematic trajectory generated in different conditions. In Table 3, the center point adds ±0.5 as the range of extension classical domain, and then the fault voltage signal is imported for fault diagnosis.

4.2. Comparison. The literature [9] simulated fault diagnosis at 1000 W/m² 25°C, so this study used 1000 W/m² 25°C, 1000 W/m² 30°C, and 900 W/m² 25°C for comparison, as shown in Tables 5(a), 5(b), 6(a), 6(b), 7(a), and 7(b).

Table 8 compares the diagnostic rates and shows the diagnostic method of the literature [9]. When the irradiance is unchanged and the temperature rises by 5°C, the diagnostic

TABLE 4: Center point values at different irradiances and temperatures.

Data	Case								
	C1	C2	C3	C4	C5	C6	C7	C8	C9
1000 W/m^2 25°C	510.4643	466.6346	403.0097	336.9965	440.9046	367.1505	392.7802	270.0989	318.5866
1000 W/m^2 30°C	423.9461	384.2504	331.8281	279.6135	360.4166	296.4365	319.305	223.3225	257.5316
1000 W/m^2 40°C	303.6795	273.2271	238.4073	203.3484	253.9672	205.7853	224.6499	162.0302	179.1338
1000 W/m^2 50°C	423.9461	384.2504	331.8281	279.6135	360.4166	296.4365	319.305	223.3225	257.5316
900 W/m^2 25°C	457.1445	423.7284	371.5272	308.6055	403.0104	340.6735	362.7715	247.7087	296.5857
900 W/m^2 30°C	386.6972	353.5165	306.1361	256.1142	333.0595	276.7268	297.0517	204.9426	240.1221
900 W/m^2 40°C	280.6887	253.7645	218.3704	186.4827	236.5171	192.9238	209.3046	148.5407	167.4806
900 W/m^2 50°C	210.7214	189.524	165.4722	141.7511	144.5628	141.4557	154.9977	112.7255	122.8688
800 W/m^2 25°C	391.5921	370.5262	333.048	280.6498	356.0653	308.557	326.1221	223.9556	272.0152
800 W/m^2 30°C	341.6574	316.5865	278.4199	231.5121	300.314	253.4934	270.7338	185.3674	221.2131
800 W/m^2 40°C	253.9414	231.2014	200.1783	168.4703	216.3469	178.0942	192.5487	134.2771	154.3977
800 W/m^2 50°C	192.0345	173.5387	150.5305	127.9922	161.1028	130.758	142.5223	101.6299	113.2707
700 W/m^2 25°C	314.5517	304.8765	284.1958	248.2921	297.1806	267.8527	279.592	199.9536	241.466
700 W/m^2 30°C	286.7018	271.0453	244.428	207.0795	259.892	225.1551	238.491	164.6638	199.2278
700 W/m^2 40°C	222.272	204.5738	179.3767	149.4428	192.5778	160.7518	172.9791	119.1263	140.088
700 W/m^2 50°C	170.4388	155.0974	134.6042	113.3157	118.4572	118.4572	128.6777	89.93955	102.556
600 W/m^2 25°C	233.7565	230.7093	223.2524	205.8939	227.9525	215.5746	221.084	174.1138	201.5134
600 W/m^2 30°C	222.609	215.5159	201.5031	177.5427	209.7437	189.2676	197.7411	144.0344	171.6018
600 W/m^2 40°C	184.113	172.3014	154.2809	130.2548	163.7463	139.8199	149.3071	103.04	123.3908
600 W/m^2 50°C	145.0369	133.3973	117.3126	97.81224	125.1117	104.0237	112.428	77.50333	90.74045
500 W/m^2 25°C	159.2883	158.5788	156.8393	152.0567	157.8894	154.6332	156.2005	138.8777	150.2812
500 W/m^2 30°C	156.1902	154.0336	149.3204	139.0552	152.0642	144.0444	147.6893	119.561	135.6136
500 W/m^2 40°C	139.2521	133.2785	123.1959	107.7763	128.4807	113.8041	119.9614	86.82071	102.6594
500 W/m^2 50°C	114.9432	107.4587	96.52619	81.99123	101.7915	86.67798	92.8941	64.3971	76.65465
400 W/m^2 25°C	97.18495	97.04757	96.744	95.95195	96.91125	96.31457	96.61014	93.35858	95.54372
400 W/m^2 30°C	96.67736	96.20672	95.20266	92.80305	95.74832	49.29442	49.44406	48.24918	48.96747
400 W/m^2 40°C	91.52255	89.52814	85.85849	79.17138	87.73116	81.62739	84.39876	67.59447	76.26249
400 W/m^2 50°C	80.47037	76.90738	71.29433	62.91227	73.94753	65.43214	69.12599	51.00417	59.25853

Table 5: 1000 W/m^2 25°C diagnostic result.

(a) Original literature

Status	Case								
	C1	C2	C3	C4	C5	C6	C7	C8	C9
C1	1	−0.71277	−0.82783	−0.98066	−0.76204	−0.8813	−0.84332	−1	−0.94555
C2	−0.72198	1	−0.77112	−0.97482	−0.68079	−0.84335	−0.79216	−1	−0.92876
C3	−0.97026	−0.91917	1	−0.9819	−0.88336	−0.88328	−0.8429	−1	−0.94815
C4	−1	−0.95903	−0.88299	1	−0.93033	−0.8293	−0.86864	−0.88656	−0.81035
C5	−0.89264	−0.83442	−0.85419	−0.98472	1	−0.90089	−0.86786	−1	−0.95529
C6	−1	−0.93853	−0.82443	−0.91072	−0.89546	1	−0.80291	−0.93911	−0.85451
C7	−0.98944	−0.92881	−0.81628	−0.97739	−0.88633	−0.84873	1	−1	−0.93314
C8	−1	−0.92787	−0.79398	−0.75559	−0.87732	−0.69945	−0.76872	1	−0.53752
C9	−1	−0.94868	−0.85341	−0.8261	−0.91271	−0.78616	−0.83544	−0.78829	1

(b) This paper

Status	Case								
	C1	C2	C3	C4	C5	C6	C7	C8	C9
C1	1	−1	−0.98248	−0.97801	−0.98897	−0.97954	−0.98146	−0.976	−0.97732
C2	−0.47293	1	−0.62539	−0.88383	−0.25053	−0.79562	−0.68466	−1	−0.92394
C3	−0.89219	−0.62946	1	−0.64614	−0.40071	−0.37748	−0.0395	−1	−0.76833
C4	−1	−0.89251	−0.60889	1	−0.80349	−0.28261	−0.5355	−0.61376	−0.1127
C5	−0.62227	−0.20589	−0.35382	−0.79961	1	−0.64747	−0.45607	−1	−0.8688
C6	−1	−0.82528	−0.36424	−0.29859	−0.68056	1	−0.24494	−0.81261	−0.48768
C7	−0.97836	−0.73257	−0.07283	−0.59351	−0.52725	−0.28489	1	−1	−0.73387
C8	−0.97527	−0.97663	−0.98023	−0.99133	−0.97776	−0.98436	−0.98115	1	−1
C9	−1	−0.9291	−0.74203	−0.16318	−0.87039	−0.52683	−0.69363	−0.52549	1

Table 6: 1000 W/m^2 30°C diagnostic result.

(a) Original literature

Status	Case								
	C1	C2	C3	C4	C5	C6	C7	C8	C9
C1	−0.12676	0.535734	0.893778	−0.16441	1	0.280185	0.713481	−1	−0.42615
C2	−1	−0.37627	0.781551	0.200473	0.060822	0.796451	1	−0.88258	−0.1439
C3	−1	−0.63702	0.036782	1	−0.38265	0.512455	0.163909	0.131216	0.844341
C4	−1	−0.75659	−0.30474	0.341188	−0.58601	0.014244	−0.21949	1	0.560711
C5	−1	−0.52001	0.370992	0.683991	−0.18365	1	0.539099	−0.35383	0.350138
C6	−1	−0.68808	−0.10905	0.718689	−0.46948	0.29972	0.000199	0.927234	1
C7	−1	−0.93896	−0.82566	−0.66369	−0.89619	−0.74567	−0.80428	−0.75234	1
C8	−1	−0.79017	−0.40065	0.156169	−0.64312	−0.12567	−0.32716	1	0.345408
C9	−1	−0.79017	−0.40065	0.156169	−0.64312	−0.12567	−0.32716	1	0.345408

(b) This paper

| Status	Case								
	C1	C2	C3	C4	C5	C6	C7	C8	C9
C1	1	−1	−0.98075	−0.97562	−0.98721	−0.97681	−0.97904	−0.9731	−0.97443
C2	−0.50963	1	−0.62158	−0.87545	−0.30151	−0.81663	−0.7059	−1	−0.93444
C3	−0.91719	−0.63621	1	−0.63327	−0.37768	−0.46009	−0.13406	−1	−0.80697
C4	−1	−0.87978	−0.58433	1	−0.77377	−0.14027	−0.46523	−0.61615	−0.22971
C5	−0.67223	−0.26196	−0.32826	−0.77891	1	−0.6745	−0.47794	−1	−0.88363
C6	−1	−0.83391	−0.42575	−0.16331	−0.68747	1	−0.26122	−0.74861	−0.46405
C7	−1	−0.75352	−0.1478	−0.51948	−0.5362	−0.30847	1	−0.95434	−0.72744
C8	−0.96412	−0.96588	−0.97019	−0.9827	−0.96743	−0.97668	−0.97193	1	−1
C9	−1	−0.93576	−0.77789	−0.32037	−0.87912	−0.54062	−0.71426	−0.48932	1

(a) P-V

(b) I-V
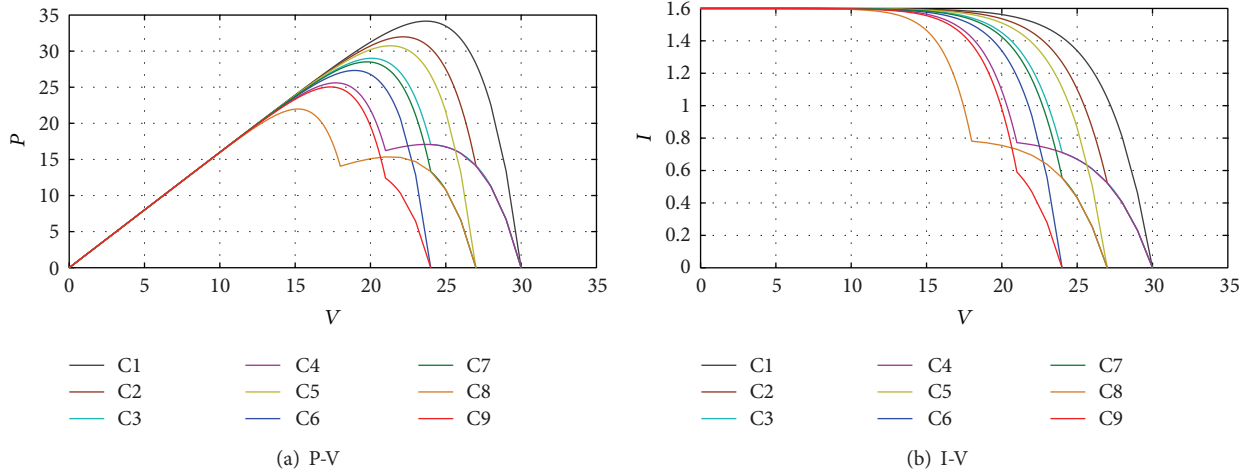
FIGURE 8: P-V and I-V characteristic curves at 1000 W/m^2 25°C.
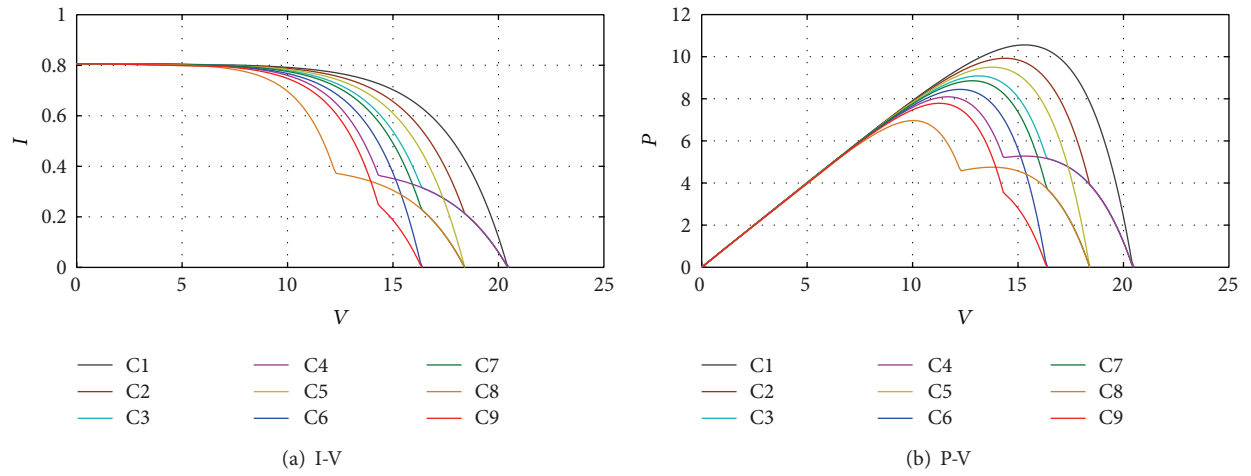

(a) I-V

(b) P-V

FIGURE 9: P-V and I-V characteristic curves at 500 W/m^2 40°C.
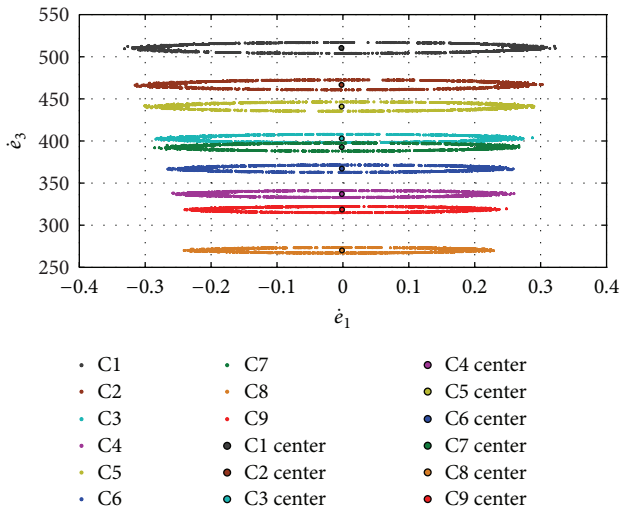

FIGURE 10: $\dot{e}_1 - \dot{e}_3$ dynamic error plane and center of different faults at 1000 W/m^2 25°C.
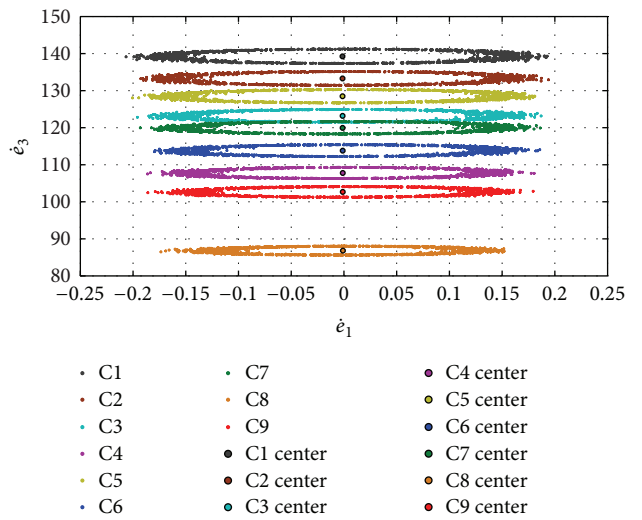
FIGURE 11: $\dot{e}_1 - \dot{e}_3$ dynamic error plane and center of different faults at 500 W/m^2 40°C.

TABLE 7: 900 W/m^2 25°C diagnostic result.

(a) Original literature

Status	Case								
	C1	C2	C3	C4	C5	C6	C7	C8	C9
C1	0.39087	1	0.35864	−0.39016	0.900709	−0.07243	0.23286	−1	−0.57939
C2	−0.13222	0.533484	0.909789	−0.15757	1	0.290808	0.727889	−1	−0.42149
C3	−1	−0.69818	−0.1379	−0.17831	−0.48667	1	−0.03219	−0.76564	−0.36617
C4	−1	−0.68808	−0.10905	0.718689	−0.46948	0.29972	0.000199	0.555377	1
C5	−0.97245	−0.92459	1	−0.92894	−0.89105	−0.89051	−0.85263	−1	−0.95137
C6	−1	−0.87885	−0.65397	1	−0.79396	−0.49521	−0.61154	−0.695	−0.47851
C7	−1	−0.76003	−0.31456	−0.19902	−0.59186	1	−0.23051	−0.70642	−0.36204
C8	−1	−0.79017	−0.40065	0.156169	−0.64312	−0.12567	−0.32716	1	0.345408
C9	−1	−0.68808	−0.10905	0.718689	−0.46948	0.29972	0.000199	0.921613	1

(b) This paper

Status	Case								
	C1	C2	C3	C4	C5	C6	C7	C8	C9
C1	1	−1	−0.97775	−0.97193	−0.98589	−0.9741	−0.97647	−0.96965	−0.97134
C2	−0.42441	1	−0.60899	−0.88998	−0.21619	−0.7852	−0.67089	−1	−0.91837
C3	−0.81912	−0.57699	1	−0.66532	−0.35669	−0.34659	0.00116	−1	−0.75167
C4	−1	−0.90157	−0.64017	1	−0.81906	−0.34539	−0.5728	−0.6241	−0.0134
C5	−0.56918	−0.16613	−0.32758	−0.8108	1	−0.63062	−0.43403	−1	−0.85962
C6	−1	−0.82945	−0.37656	−0.38985	−0.68651	1	−0.25984	−0.88577	−0.52306
C7	−0.89864	−0.67586	−0.03513	−0.61682	−0.48165	−0.25189	1	−1	−0.71569
C8	−0.97645	−0.97778	−0.98132	−0.99383	−0.9789	−0.9853	−0.98223	1	−1
C9	−1	−0.92758	−0.73526	−0.05418	−0.86688	−0.51838	−0.6857	−0.56027	1

TABLE 8: Comparison of diagnostic rates.

State	Category	
	Diagnostic rate in literature [9]	Diagnostic rate in this paper
1000 W/m^2 25°C	100%	100%
1000 W/m^2 30°C	11.11%	100%
900 W/m^2 25°C	22.23%	100%

rate decreases to 22.23% as the range of chaotic kinematic trajectory is changed. When the irradiance decreases to 1000 W/m^2 and the temperature is unchanged, the diagnostic rate is only 11.11%. The diagnostic rate will decrease greatly if the temperature or irradiance changes.

5. Conclusion

The chaotic extension neural network diagnosis proposed in this paper is integrated with error backpropagation neural network. It can remedy the defect of large decrease in diagnostic rate when the irradiance and temperature have changed in the original literature effectively. The defect in the original literature is remedied, and the high diagnostic rate in the original literature is maintained. In comparison to the original neural network diagnosis, the addition of extension theory reduces the time of repeated training. In addition, as the chaos synchronization theory is used, when the diagnosis is difficult due to undervoltage caused by the environment, the signal can be amplified by using the advantages of chaos theory for diagnosis.

Conflict of Interests

The authors declare that there is no conflict of interests regarding the publication of this paper.

References

[1] M. Rizwan, M. Jamil, and D. P. Kothari, "Generalized neural network approach for global solar energy estimation in india," *IEEE Transactions on Sustainable Energy*, vol. 3, no. 3, pp. 576–584, 2012.

[2] H. A. Talebi and K. Khorasani, "A neural network-based multiplicative actuator fault detection and isolation of nonlinear systems," *IEEE Transactions on Control Systems Technology*, vol. 21, no. 3, pp. 842–851, 2013.

[3] S. Yousef and A. K. Mahmood, "Fault diagnosis in internal combustion engines using extension neural network," *IEEE Transactions on Industrial Electronics*, vol. 61, no. 3, pp. 1434–1443, 2014.

[4] Y. Wu, Q. Lan, and Y. Sun, "Application of BP neural network fault diagnosis in solar photovoltaic system," in *Proceedings of the IEEE International Conference on Mechatronics and Automation (ICMA '09)*, pp. 2581–2585, Changchun, China, August 2009.

[5] S. Syafaruddin, E. Karatepe, and T. Hiyama, "Controlling of artificial neural network for fault diagnosis of photovoltaic array," in *Proceedings of the 16th International Conference on Intelligent System Applications to Power Systems (ISAP '11)*, Hersonissos, Greece, September 2011.

[6] T. Shimakage, K. Nishioka, H. Yamane, M. Nagura, and M. Kudo, "Development of fault detection system in PV system," in *Proceedings of the IEEE 33rd International Telecommunications Energy Conference (INTELEC '11)*, pp. 1–5, Amsterdam, The Netherlands, October 2011.

[7] Y. Zhao, L. Yang, B. Lehman, J.-F. de Palma, J. Mosesian, and R. Lyons, "Decision tree-based fault detection and classification in solar photovoltaic arrays," in *Proceedings of the 27th Annual IEEE Applied Power Electronics Conference and Exposition (APEC '12)*, pp. 93–99, Orlando, Fla, USA, February 2012.

[8] M. Tadj, K. Benmouiza, A. Cheknane, and S. Silvestre, "Improving the performance of PV systems by faults detection using GISTEL approach," *Energy Conversion and Management*, vol. 80, pp. 298–304, 2014.

[9] C.-T. Hsieh, H.-T. Yau, and J. Shiu, "Chaos synchronization based novel real-time intelligent fault diagnosis for photovoltaic systems," *International Journal of Photoenergy*, vol. 2014, Article ID 759819, 9 pages, 2014.

[10] C.-H. Huang, C.-H. Lin, and C.-L. Kuo, "Chaos synchronization-based detector for power-quality disturbances classification in a power system," *IEEE Transactions on Power Delivery*, vol. 26, no. 2, pp. 944–953, 2011.

[11] K.-H. Chao, S.-H. Ho, and M.-H. Wang, "Modeling and fault diagnosis of a photovoltaic system," *Electric Power Systems Research*, vol. 78, no. 1, pp. 97–105, 2008.

[12] M. H. Wang and H. H. Tsai, "Fuel cell fault forecasting system using grey andextension theories," *IET Renewable Power Generation*, vol. 6, no. 6, pp. 373–380, 2012.

[13] K.-H. Chaoa, S.-H. Hob, and M.-H. Wang, "Application of extension theory to vibration fault diagnosis of generator sets," *Electric Power Systems Research*, vol. 78, no. 1, pp. 97–105, 2008.

[14] L. Boukezzi and A. Boubakeur, "Prediction of mechanical properties of XLPE cable insulation under thermal aging: neural network approach," *IEEE Transactions on Dielectrics and Electrical Insulation*, vol. 20, no. 6, pp. 2125–2134, 2013.

[15] C. Y. Chang, C. J. Li, and C. W. Cheng, "Application of hybrid solar light collectors and artificial light sources on interior lighting," *Journal of Design*, vol. 16, no. 2, pp. 45–60, 2011.